Deformation of a Polydomain, Smectic Liquid Crystalline Elastomer

C. Ortiz,[†] M. Wagner,[‡] N. Bhargava, C. K. Ober,* and E. J. Kramer[§]

Cornell University, Department of Materials Science and Engineering and The Materials Science Center, Bard Hall, Ithaca, New York 14853

Received September 25, 1997; Revised Manuscript Received August 12, 1998

ABSTRACT: A main-chain, polydomain, smectic liquid crystalline elastomer (LCE) was prepared by reacting the LC epoxy monomer, diglycidyl ether of 4,4′-dihydroxy-α-methylstilbene, with the aliphatic diacid, sebacic acid. When deformed in uniaxial tension, a "polydomain-to-monodomain" transition took place leading to bulk, macroscopic orientation. With this process was associated a plateau in the nominal stress-versus-strain curve and a dramatic change in optical properties from opaque to translucent. Polarized optical microscopy showed that the transition took place by an elongation of the LC domains and a rotation of the local director orientations along the stress axis. The strain and orientation of the deformed samples were retained upon unloading, even after annealing above T_g for extended periods. Upon heating, the oriented LCEs disordered at the same temperature as the undeformed polydomains and "remembered" their original polydomain microstructure and sample dimensions when subsequently cooled from the isotropic state.

Introduction

Liquid Crystalline Elastomers (LCEs) are loosely cross-linked networks that have rigid-rod, LC molecules incorporated directly into the polymer backbone (i.e., "main-chain" LCEs) or attached to the polymer backbone via a flexible spacer group (i.e., "side-chain" LCEs). These materials typically have low glass transition temperatures (T_g < 35 °C) and low moduli ($E \approx 0.5$ MPa), deform at nearly constant volume, and exhibit liquid crystalline phase transitions due to the high mobility of the network strands. The networks used in this study were ordered locally into a smectic phase, on a scale less than 1 μm; i.e., the molecules exhibited orientational order along a unit vector called the director, $\hat{n}$, in addition to positional order in two-dimensional planes or sheets (Figure 1a). On a larger scale (>1 μm), the LCEs exhibited both a continuous reorientation of $\hat{n}$ as well as abrupt discontinuities in $\hat{n}$, line defects called *disclinations***.** This unique isotropic "polydomain" microstructure (Figure 1b) results in a finely scaled *Schlieren* texture,[1] when viewed under the polarizing optical microscope. These brushes emanate from disclinations and are visible where $\hat{n}$ is oriented along the polarizer or analyzer axes. The characteristic length scale of the texture or LC "domain size" can be approximated by the mean distance between disclinations, and since this parameter is typically about the wavelength of light, the material appears opaque in bulk form.

The unique properties of LCEs[2,3] originate from the coupling between an applied mechanical stress and the LC director(s). One of the most remarkable characteristics is the ability to undergo a polydomain-to-monodomain transition; i.e., stress-induced macroscopic orientation leading to the formation of a "liquid single-crystal elastomer." The average degree of orientation of the LC domains with respect to the tensile direction can be represented by the orientation parameter, S, which is defined according to eq 1:

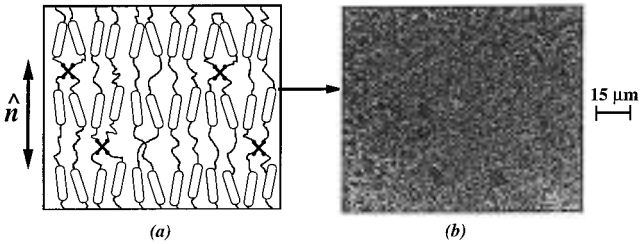

Figure 1. A liquid crystalline elastomer with (a) smectic type local order and a (b) polydomain microstructure (as viewed under the polarizing optical microscope).

$$S = \frac{3\langle \cos^2 \varphi \rangle - 1}{2} \tag{1}$$

where φ is the angle between the individual domain directors, $\hat{n}$, and the tensile direction and < > denotes an average of $\cos^2\varphi$ over all the LC domains. $S = 1$ for a perfectly uniaxially oriented sample; $S = 0$ for a completely random, isotropic sample; and $S = -0.5$ for a planar orientation.

The polydomain-to-monodomain transition is a well-known, universal phenomenon and has been reported for side-chain LCEs based on siloxanes,[4,5] side-chain polyacrylate and polymethacrylate networks, a main-chain polymalonate, a combination of these to form side-chain/main-chain networks,[6−18] a main-chain, epoxide-based network,[19] and main-chain, semirigid, epoxide-based networks.[20,21] Most experimental work to date has focused on side-chain, nematic LCEs. In 1989, Schätzle et al.[10] conducted uniaxial tensile experiments on a side-chain, nematic, methacrylate-based elastomer just below the nematic-to-isotropic ("clearing") transition temperature. They found a three-region nominal stress-versus-nominal strain curve and a unique relationship between orientation parameter, S, and nominal stress (Figure 2).

[†] Current address: Department of Polymer Chemistry, University of Groningen, Nijenborgh 4, 9747 AG Groningen, The Netherlands.

[‡] Current address: Fachbereich Chemie und Pharmazie, Universität Mainz, 55099 Mainz.

[§] Current address: Materials Department, University of Santa Barbara, Santa Barbara, California 93106-5050.

10.1021/ma971423x CCC: $15.00
Published on Web 11/10/1998

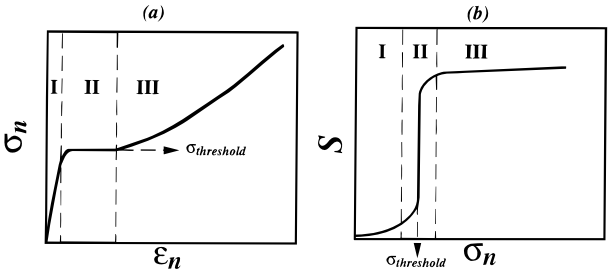

Figure 2. Schematic of (a) nominal stress-versus-nominal strain curve and (b) orientation parameter-versus-nominal stress of a polydomain LCE; region (I) is the linear elastic deformation of the polydomain, region (II) is the polydomain-to-monodomain transition, and region (III) is the deformation of the monodomain.

Region I: At small strains, the polydomain elastomer deformed in a linear elastic manner with a typical rubber modulus, corresponding to a small nonlinear increase in the orientation of the material with nominal stress.

Region II: At intermediate strains, a reversible polydomain-to-monodomain transition took place in which the sample was converted from turbid to optically transparent, and the mesogens became aligned parallel to the stress axis. The transparency of the sample is thought to result from the strong suppression of thermal fluctuations of the director by coupling to the network.[3] The transition led to a plateau in the stress-versus-strain curve and corresponded to a dramatic increase in S at a critical threshold stress, $\sigma_{\text{threshold}}$. The drop in apparent elastic modulus in this region was attributed to chain relaxation during local director reorientation.[22]

Region III: At large strains, the modulus increased again (although to a different value), and only a small amount of additional orientation was achieved.

The stress-induced molecular orientation could be "frozen in" by cooling the sample below the glass transition while retaining the applied stress. When stretching was done in the isotropic state, the plateau in the stress-versus-strain curve was absent, and the orientation induced by the same strain was much smaller. This corresponds to the situation in non-LC elastomers, for which strains up to 1000% are necessary to achieve considerable orientation.

There is much speculation on exactly how the polydomain-to-monodomain transition takes place.[22−26] Theoretical formulations of side-chain LCEs are difficult because the backbone/mesogen coupling may depend on several factors; e.g., the number of units in the attaching polymer chain[6] and the stiffness of the backbone.[7] Main-chain LCE systems are much more straightforward and convenient to analyze. Hence, we have chosen to use the main-chain, smectic, epoxide-based LCE reported in ref. 19 in this study. In the first section of this article, we explore the mechanical behavior in uniaxial tension over a broad temperature range. One great advantage of the network used in this study is that it possesses large enough LC domains to allow us to observe the in situ response to a mechanical field under the polarizing optical microscope. We also describe our observations of domain deformation and reorientation and quantify these results using image analysis techniques. Last, we discuss the results of dynamic mechanical analysis on unoriented and oriented samples. We feel that these experiments will provide a more concrete basis for theoretical comparison and also give clues to recent findings on increased fracture toughness in smectic LC thermosetting networks.[27,28]

Experimental Section

Characterization Techniques. The monomer composition was determined by NMR using a Varian XL-200 ^{1}H NMR and Fourier transform infrared spectroscopy using a Galaxy Series 2020 FTIR with 64 scans at a resolution of 4 cm^{-1} in KBr. Differential scanning calorimetry (DSC) was performed using a Perkin-Elmer DSC-7 at a heating/cooling rate of 10 °C/min under continuous nitrogen flow to determine thermal transition temperatures. Decomposition temperatures were measured using thermogravimetric analysis on a Perkin-Elmer TGA-7 at a heating/cooling rate of 10 °C/min. Liquid crystalline textures were examined using a Nikon Optiphot-2 polarizing optical microscope (POM) model 284678 equipped with a Mettler FP-82 HT hot stage (heating/cooling rate of 10 °C/min), Mettler FP-80 temperature controller, photomonitor, and Canon AE1 35-mm camera. A Scintag X-ray generator was used to carry out wide-angle X-ray diffraction (WAXD) experiments. The generator was operated at 40 mA and 45 kV and produced copper $K_{\alpha 1}$ X-rays with a wavelength of 1.54051 Å. The X-rays traveled through a pinhole collimator into a Statton flat film camera equipped with a heater that was connected to a calibrated temperature controller. The sample-to-film distance was 49 mm. A flat film cartridge containing Kodak DEF-5 film was exposed for 4−8 h. The setup is shown schematically in the appendix (Figure 22). The orientation parameter, S, of the mechanically deformed samples was calculated from WAXD patterns as described in the Appendix, Section 1.

The LC Monomer, Curing, and Network Characterization. The liquid crystalline epoxy monomer used in this study, diglycidyl ether of 4,4′-dihydroxy-α-methylstilbene (DGDHMS), was synthesized in a manner similar to ref. 29. The procedure is described in the Appendix, Section 2. Characterization was accomplished via thin-layer chromatography (TLC), FTIR, and ^{1}H NMR. DSC and POM results showed that the DGDHMS is a monotropic nematogen which exhibits an LC phase upon cooling from the isotropic melt at T_{IN} = 106 °C. The monomer was mechanically mixed with decanedioic (sebacic) acid (SA, 98% purity, Aldrich Chemical Co.) in a molar ratio of 1:1.[19] The finely ground mixture was placed in a glass mold, which had been previously coated in a 3 mM solution of octadecyltrichlorosilane in 80%/20% hexadecane/carbon tetrachloride to provide a nonreactive, nonstick coating and then cured in the isotropic phase of the mixture at 180 °C for 1.5 h.

Figure 3 outlines the proposed reaction mechanism[19] for the reaction between DGDHMS and sebacic acid. The first reaction is an epoxide esterification reaction and involves opening of the epoxy ring by the carboxyl group. The resulting hydroxy groups can then undergo a condensation esterification with excess carboxylic acid molecules or through a homopolymerization etherification reaction with unreacted epoxy molecules (where proton donors can catalyze the reaction). The prevailing reaction path is not clear.[30] The FTIR spectrum of the cross-linked network (Figure 4) shows the complete disappearance of the epoxide ring stretching band (918 cm^{-1}) as well as the appearance of the ester stretching C═O band (1734 cm^{-1}) and the −OH stretching band (3450 cm^{-1}). The network was found to have a decomposition temperature of approximately 418 °C by thermogravimetric analysis.

DSC scans of the elastomer (Figure 5) show that the network possesses a glass transition temperature of ≈36 °C and a broadened clearing transition, T_i (LC to isotropic phase transition), relative to the DGDHMS monomer, at ≈98 °C on heating. When observed under the polarizing optical microscope, the networks exhibit a Schlieren texture (Figure 1b) with larger domains than those observed in the fine-grained texture of densely cross-linked DGDHMS-based thermosets.[20,27] A WAXD pattern of the network (Figure 6) displays two uniform rings typical of an unoriented, polydomain

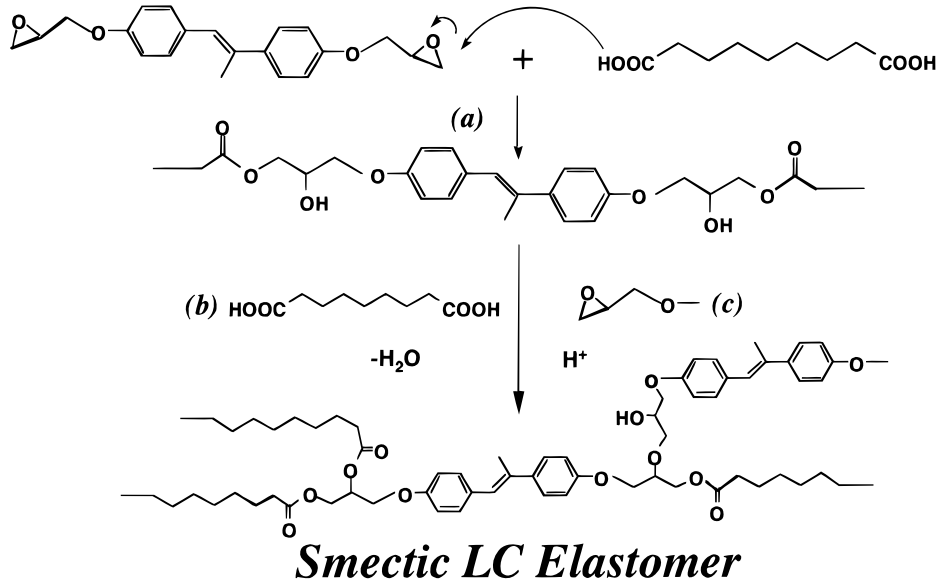

Figure 3. Cross-linking reaction of DGDHMS with sebacic acid: (a) epoxide esterification reaction, (b) condensation\esterification reaction, and (c) etherification reaction.

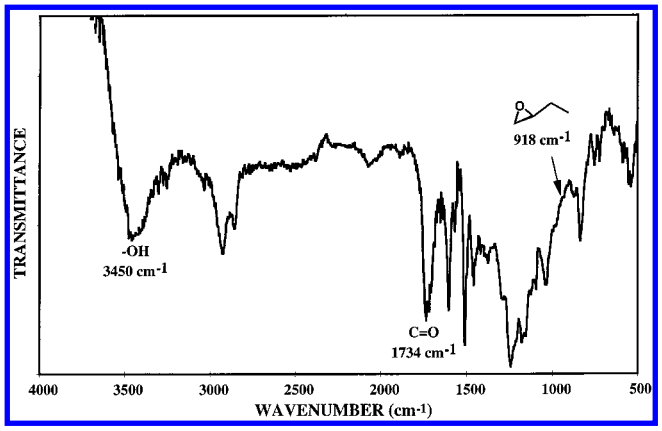

Figure 4. FTIR spectrum (KBr) of the network formed from DGDHMS and sebacic acid.

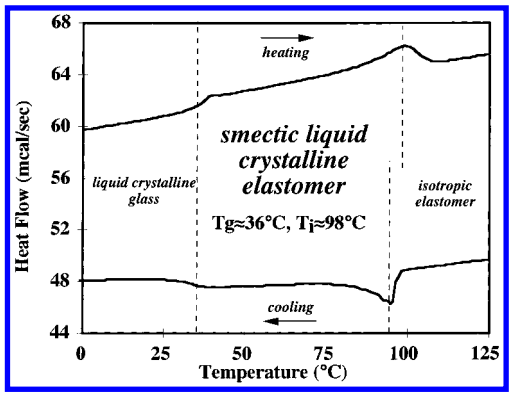

Figure 5. DSC scans of the network formed from DGDHMS and sebacic acid.

sample. The sharp, inner ring corresponds to the distance between smectic layers (d = 14.5 Å), and the diffuse outer ring corresponds to the lateral spacing between the mesogens (d = 4.3 Å).

For comparison, experiments were also performed on cross-linked polyisoprene samples prepared in the following manner. Polyisoprene (84 wt %), sulfur (3.9 wt %), "Altax" accelerator (3.9 wt %), and "Age-Rite" (inhibits high-temperature degradation, 7.7 wt %) were masticated and cured at 175 °C under pressure for 15 min. The T_g of the network was approximately −60 °C.

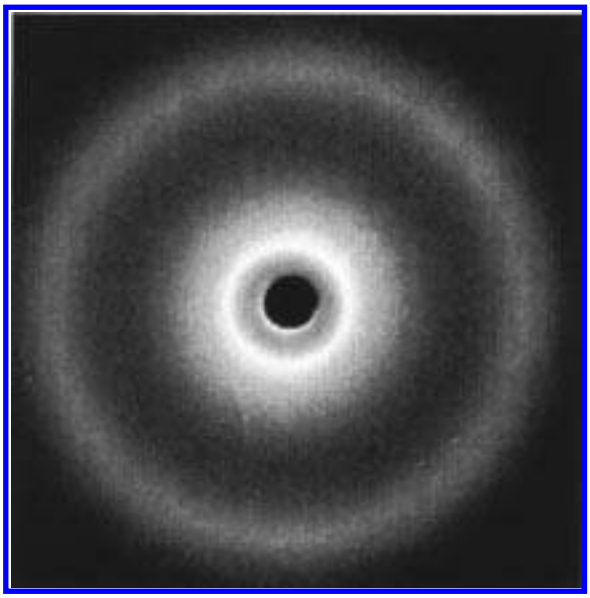

Figure 6. WAXD pattern of the network formed from DGDHMS and sebacic acid where $\boldsymbol{k} = 2\sin\theta_B/\lambda$, where $\boldsymbol{k}$ is the reciprocal space scattering vector, θ_B is the Bragg angle, λ is the wavelength of the incident X-ray beam, ≈1.54 Å.

Uniaxial Tension. Experiments were performed on 0.25 cm × 0.1 cm × 1 cm samples using an Instron (model 1125) mechanical testing machine equipped with a CCF A20 lb load cell at a displacement rate 0.5 cm/min. Temperature control was achieved with an environmental chamber and temperature controller (Applied Test Systems MTF 310). Force, F, versus displacement, δ, data were converted into nominal stress, σ_n, versus nominal strain, ϵ_n.

Stress-Optical Experiments. A minimechanical tester was connected to a stepper motor (Motomatic, Electrocraft Corp.) and strain controller (Electrocraft Corp, Model E-552-S) set at 0.25 Krpm (displacement rate, $d\delta/dt$ = 0.5 cm/min). Straining was conducted in uniaxial tension (gauge length, L_o ≈0.4 cm) under the polarizing optical microscope at 45° to the polarizer or analyzer axes. Temperature control (±2 °C) was achieved with a hot-air gun connected to a Digi-Sense temperature controller (Cole-Parmer Instruments) and type K thermocouple which was placed adjacent to the sample. The sample area, hot-air gun, thermocouple, and objective lenses were enclosed in aluminum foil to minimize temperature

gradients and background light. A Mettler photomonitor was connected to a Mettler FP82HT hot stage and automatically recorded light intensity, I, versus time, t, which was then converted into nominal strain ($\epsilon_n = [t\bullet(d\delta/dt)]/L_o$) and subsequently nominal stress (by comparison with the stress-versus-strain data obtained using the Instron mechanical tester). The degree of macroscopic orientation (and hence, S) is directly related to the light intensity measured under the polarizing optical microscope at 45° to the polarizer/analyzer axes. The orientation parameter calculated from X-ray diffraction studies was used to calibrate the light intensity measurements.

Polarized Optical Microscopy. Thin films (30 μm in thickness) of the LC elastomer were prepared by curing the DGDHMS/SA between polished NaCl crystals. The crystals were floated off in a water bath yielding free-standing films which were subsequently strained under the polarized optical microscope at 45° to the polarizer/analyzer axis. Photos were taken at increasing strain values, scanned in as black and white *.tiff files, converted to binary format, and analyzed with a image analysis program written in Fortran.[31] The size distributions of the bright (oriented) domains were measured parallel and perpendicular to the stress direction. Because some of the distributions were multimodal, the average domain sizes and standard deviations were calculated manually using approximately 50 data points.

Dynamic Mechanical Analysis (DMA). The small strain dynamic mechanical behavior was investigated using a Perkin-Elmer dynamic mechanical analyzer (DMA7) in an extension mode configuration. The sample dimensions were 20 mm × 2 mm × 1 mm. The testing was carried out at a frequency, ω, of 1 Hz, a static stress of 10 kPa, a dynamic stress amplitude of 5 kPa, and a heating rate of 5 °C/min in a He atmosphere. Storage moduli (E'), loss moduli (E''), and loss tangent (tan(δ)) were recorded as a function of temperature from 20 °C to 300 °C in stress-controlled mode. The glass-to-rubbery transition temperature was recorded as the peak of the tan(δ) curve.

Results and Discussion

Uniaxial Tension. Polyisoprene: The mechanical deformation of the cross-linked polyisoprene in uniaxial tension on loading and unloading at room temperature is given in Figure 7. The large strain, nonlinear, elastic behavior, and resulting S-shaped form of the nominal stress-versus-strain curve represents behavior typical of isotropic, amorphous elastomers. A large increase in stress occurs at high extensions because of the finite extensibility of the network strands and macroscopic orientation of the network. It has been shown that classical rubber elasticity theory, using the phenomenological formulation of Mooney and Rivlin,[32] cannot accurately describe the mechanical deformation of conventional elastomers.[33,34] Recent modifications to this theory have been successful in fitting such data.[35] The nominal strain to failure, ϵ_f, for the polyisoprene was ≈250%. The rubbery shear modulus, G_R (≈1.5 MPa), can be calculated by fitting the data of Figure 7 to

$$\sigma_n = G_R(\lambda - 1/\lambda^2) \qquad (2)$$

From this fit, it is possible to estimate the degree of cross-linking with reasonable accuracy using eq 2 from classical rubber elasticity theory[32]:

$$\langle M_x \rangle = \frac{\rho R T}{G_R} \qquad (3)$$

where $\langle M_x \rangle$ is the average molecular weight between cross-links, ρ is the density of the network, T is the absolute temperature (K), and R is the universal gas constant. The result is a value of $\langle M_x \rangle$ ≈3000 g/mol. Another characteristic of isotropic, amorphous elastomers is the presence of a small amount of mechanical hysteresis (i.e., the unloading curve does not follow exactly the same path as the loading curve). The area between the two curves is equivalent to the amount of energy per unit volume dissipated during the deformation cycle.

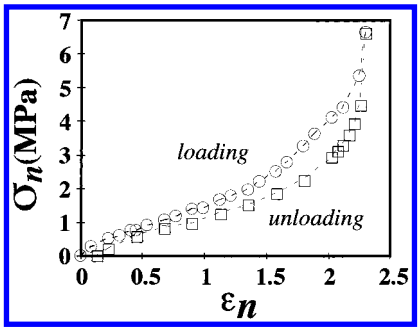

Figure 7. Nominal stress versus nominal strain for polyisoprene elastomer in uniaxial tension on loading (○) and unloading (□).

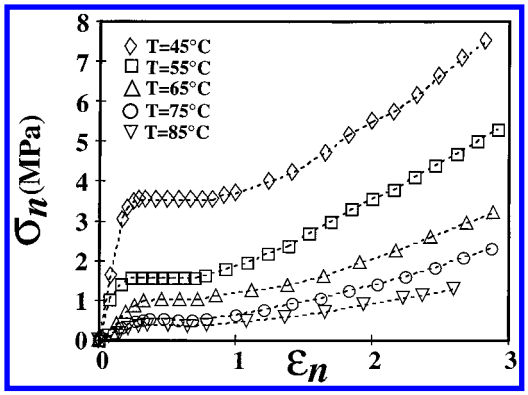

Figure 8. Nominal stress-versus-nominal strain curves for the DGDHMS/SA LCE in the smectic phase.

LC Elastomer: Figure 8 shows the nominal stress-versus-nominal strain curves for the LC elastomer at a series of temperatures within the smectic phase; the LC elastomer appears very different from the polyisoprene. In general, the smectic LCE exhibits a three-region plot similar to that described in the introduction for nematic, side-chain elastomers. At small ϵ_n (region I), there is a linear elastic increase in stress with strain, giving the elastic modulus of the polydomain. At intermediate ϵ_n (region II), the curve becomes nonlinear and then quickly exhibits a plateau region from ϵ_n ≈10%−100%. At this point, the initially turbid samples become optically translucent, indicative of a polydomain-to-monodomain transition. The translucency of sample suggests that orientation is not complete. The transition begins at the center of the gauge length and slowly propagates toward the grips. A narrowing of the sample cross-sectional area is observed (corresponding to an extension along the stress axis) in the region where the transition has taken place. Similar to the process of "necking" in many amorphous, glassy polymers, this inhomogeneous deformation is thought to be one of the primary factors contributing to stress plateau. At large ϵ_n (region III), the stress begins to increase again with increasing ϵ_n (i.e., this is the flow stress of the oriented sample) until failure ensues at ϵ_n ≈300%. The same temperature dependence is observed as for the nematic side-chain elastomers,[8,9] i.e., a dramatic decrease in the critical threshold stress and Young's modulus with increasing temperature from σ_n = 3.5 MPa, E = 16.5

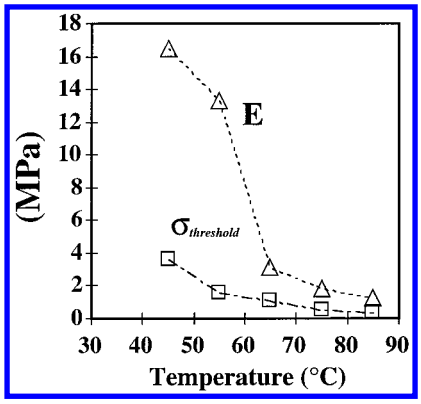

Figure 9. Modulus, E, and threshold stress, $\sigma_{threshold}$, as a function of temperature for the DGDHMS/SA polydomain, smectic LCE.

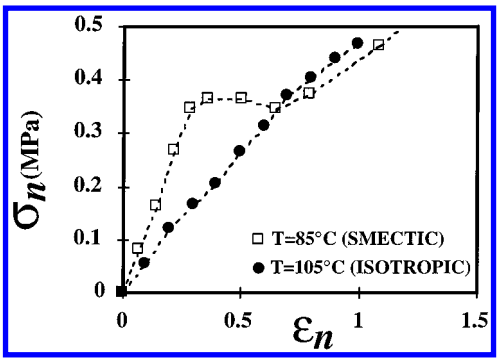

Figure 10. Nominal stress versus nominal strain for the DGDHMS/SA LC elastomer in the isotropic compared with the smectic phase.

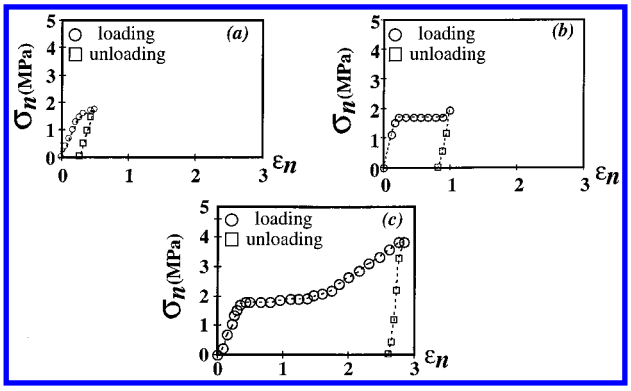

Figure 11. Mechanical hysteresis of the DGDHMS/SA LC elastomer in the smectic phase (T = 55 °C). Samples were loaded up to nominal strains of (a) ≈40%, (b) ≈90%, and (c) ≈290%.

MPa (45 °C) to σ_n = 0.4 MPa, E = 1.2 MPa (85 °C), as shown in Figure 9.

Figure 10 compares the deformation behavior of the elastomer in the smectic phase with that in the isotropic phase. It is interesting to note the absence of the plateau in the isotropic phase and also the dramatic decrease in nominal strain-to-failure (ϵ_f < 100% for the isotropic phase). By fitting eq 2 to the data of Figure 10, we obtained a value of G_R ≈0.24 MPa, which yields a value of $\langle M_x \rangle$ ≈13,100 g/mol (≈20 monomers) from eq 3.

Samples were loaded up to different values of nominal strain (≈40%, 90%, and 290%) at 55 °C and then the strain direction was reversed to observe recovery on unloading. As shown in Figure 11, the samples exhibited a large mechanical hysteresis, recovering only 1%–

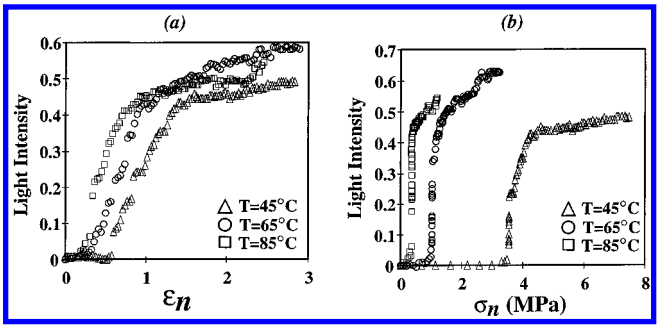

Figure 12. Light intensity measured under the polarizing optical microscope (sample positioned at 45° to the polarizer/analyzer axes) versus (a) nominal strain and (b) nominal stress for DGDHMS/SA LC elastomer in the smectic phase.

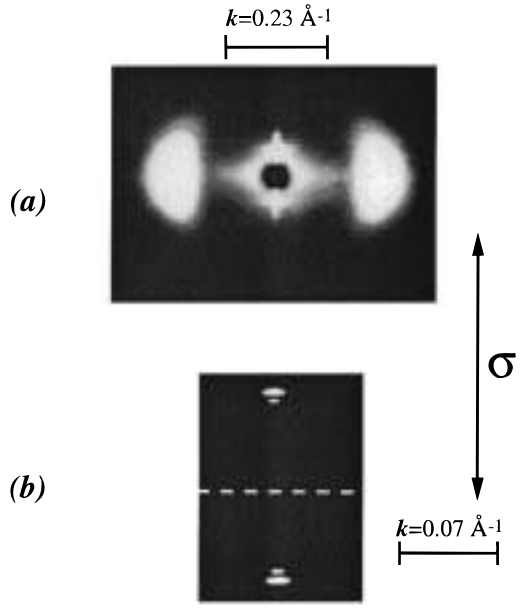

Figure 13. X-ray diffraction patterns of mechanically oriented DGDHMS/SA smectic elastomer; (a) wide-angle region and (b) small-angle region; $\boldsymbol{k} = 2\sin\theta_B/\lambda$, where $\boldsymbol{k}$ is the reciprocal space scattering vector, θ_B is the Bragg angle, λ is the wavelength of the incident X-ray beam, ≈1.54 Å.

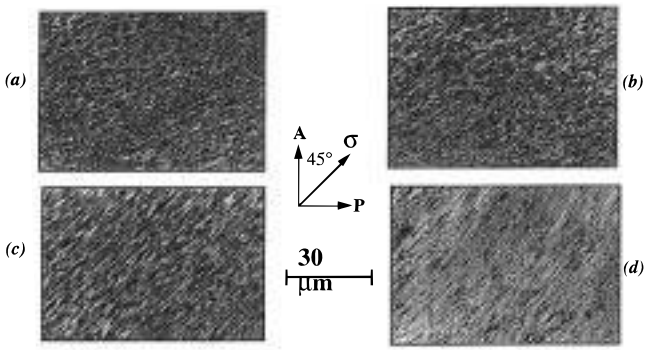

Figure 14. Variation in polydomain texture of DGDHMS/SA smectic liquid crystalline elastomer: (a) 20% nominal strain, (b) 60% nominal strain, (c) 200% nominal strain, and (d) 300% nominal strain (T = 55 °C) as viewed under the polarizing optical microscope.

2% nominal strain. On removing the samples from the grips, the orientation and strain were "frozen in" permanently, even when the sample was annealed above T_g. This behavior is reminiscent of a semicrystalline polymer between T_g and T_m, because it indeed possesses a "yield point" (the critical threshold stress), followed by plastic deformation. The large mechanical

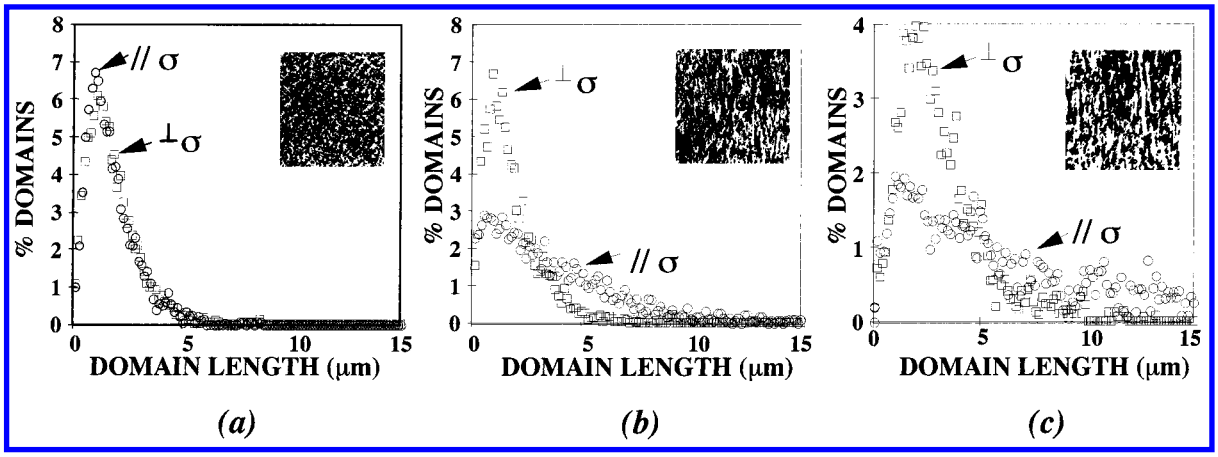

Figure 15. Distributions of LC domain lengths in smectic LCE parallel and perpendicular to stress axis: (a) 0% nominal strain, (b) 60% nominal strain, and (c) 190% nominal strain (stress axis for micrographs in inset is vertical).

hysteresis of the smectic phase could be of great technological importance because large amounts of energy dissipation during deformation typically lead to materials with extremely high fracture toughness. It may also explain the recent findings of increased fracture toughness in smectic LC thermosetting networks.[27,28] In addition, mechanical alignment of these samples can be used for easily preparing oriented smectic LCEs, similar to magnetic or electric field alignment, which can then be subjected to future experiments. On heating, the oriented elastomers exhibited a clearing transition at approximately the same temperature as the polydomain samples (98 °C) and, when subsequently cooled from the isotropic phase, recovered their original polydomain microstructure and sample dimensions.

Stress-Optical and Wide-Angle X-ray Diffraction. Figure 12 plots the increase in light intensity under the polarizing optical microscope with nominal strain and stress from the stress-optical experiments. A continual increase in light intensity (and hence, orientation) is observed with increasing nominal strain until a plateau is reached at large strains. The polydomain-to-monodomain transition shifts to lower strains with increasing temperature; from ≈100% (T = 45 °C) to ≈25% (T = 85 °C). The same data plotted against nominal stress are more dramatic; a large jump in light intensity is observed at the critical threshold stress, which shifts to lower values with increasing temperature. This is different from conventional elastomers where the relationship between orientation and stress is approximately *linear*.[31] However, this behavior is analogous to the stress-optical response of semicrystalline polymers, where the birefringence develops rapidly as a function of strain at constant stress (the yield stress).

A typical X-ray diffraction pattern of the mechanically oriented smectic elastomer (strained to failure, $\epsilon_f \approx 2.75$) is given in Figure 13 and shows orientation in both the wide-angle and small-angle regions. The molecular d spacings for the oriented samples were observed to be the same as the unstrained polydomains within experimental error. The local order was observed to stay intact upon straining. Azimuthal scans produce values of the orientation parameter, S, between 0.5 and 0.6.

Polarized Optical Microscopy. Figure 14 shows the variation in polydomain texture of the thin-film LCEs in the smectic phase as viewed under the polarized optical microscope during uniaxial tensile deformation at 55 °C and 45° to the polarizer/analyzer axes.

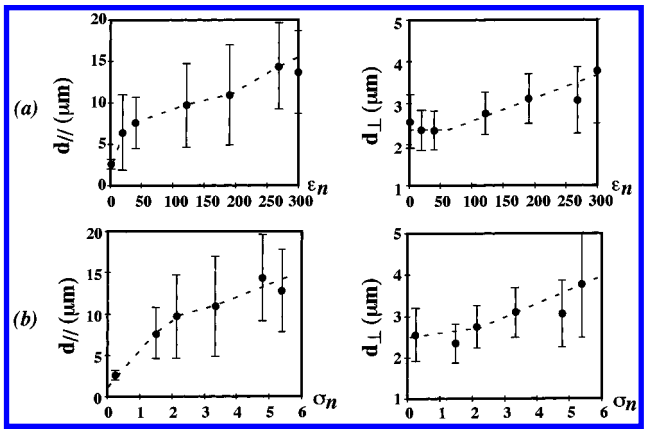

Figure 16. Domain lengths as a function of nominal strain (a) and nominal stress (b) for smectic LCE parallel and perpendicular to stress axis.

Image analysis was used to quantify these results further as shown in Figure 15. Figure 15a is a plot of the distribution of domain lengths parallel and perpendicular to the stress axis in an unstrained polydomain sample. It is clear that the sample exhibits a uniform distribution (as indicated by a low amount of scatter) which is isotropic with an average domain size of ≈2.0−3.0 μm. On straining, the distribution parallel to the stress axis broadens, changes shape (becoming multimodal), shifts to higher values, and becomes noisier. This result indicates that the domains elongate along the stress axis and that the texture becomes much more nonuniform. The distribution perpendicular to the stress axis does not change significantly until high strains, at which time it also starts to broaden slightly and becomes noisier. This point is clarified further in Figure 16, which plots the average domain size parallel, $d_{//}$, and perpendicular, $d_{\perp}$, to the stress axis as a function of nominal strain and stress. Here, the $d_{//}$ exhibits a nonlinear increase with nominal strain and stress, whereas $d_{\perp}$ shows a nearly linearly increasing trend. $d_{\perp}$ increases at a much slower rate than $d_{//}$. A higher magnification polarized optical micrograph (Figure 17) shows that even in the highly oriented samples, many defects are present running along the stress axis. Figure 18 is a schematic which illustrates the changes in texture more clearly.

Dynamic Mechanical Analysis. Recently, some work has been published on the dynamic mechanical properties of liquid crystalline elastomers.[36−38] Figures 19a−c plot the storage moduli, E', the loss moduli, E'',

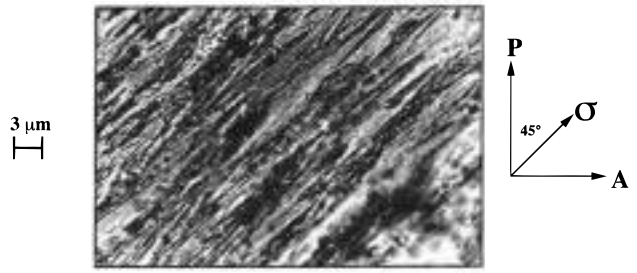

Figure 17. Polarized optical micrograph of oriented DGDHMS/SA smectic LCE (P = polarizer axis; A = analyzer axis).

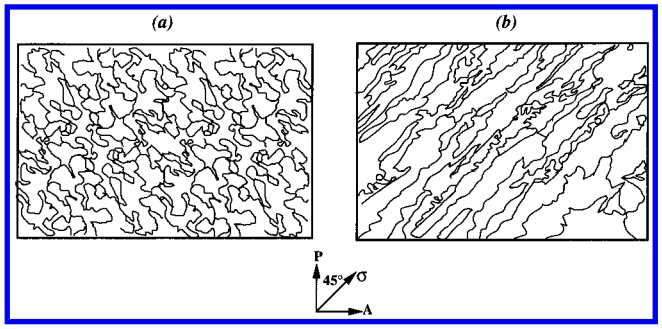

Figure 18. Schematic of the deformation an reorientation of the LC domains in a smectic LCE under the polarizing optical microscope: (a) unstrained polydomain and (b) oriented sample (P = polarizer axis; A = analyzer axis).

and the loss tangent, tan(δ), as a function of temperature for the unoriented (polydomain) and oriented ("monodomain") DGDHMS/SA LCE along the directions parallel and perpendicular to the stress axis. For the polydomain LCE, the glassy storage modulus E' ($\approx$1 GPa) exhibits a large drop near T_g to $\approx$10 MPa and a corresponding peak in the tan(δ) curve. There is also a significant drop in modulus near the clearing transition ($\approx$2.5 MPa), suggesting a large effect of liquid crystalline order. Similar to polydomain, smectic LC thermosets above T_g,[26] the smectic phase of the LCE above T_g, exhibits a modulus that decreases slowly with increasing temperature. The oriented samples are highly anisotropic. The entire curve is shifted up (to higher modulus values) for the experiments conducted parallel to the stress axis and shifted down (to lower modulus values) for the samples that were tested perpendicular to the stress axis. Also, there is a shift in peak of the tan(δ) curve for the oriented samples; by $\approx$+5 °C for the samples parallel to the stress axis and by $\approx$−5 °C for the samples tested perpendicular to the stress axis.

Literature Comparison. It is interesting to note that the mechanical behavior of the epoxide-based, main-chain, smectic LCE used in this study is qualitatively similar to that of the nematic, side-chain LCEs, suggesting that the polydomain-to-monodomain transition is a universal phenomenon. However, a quantitative comparison (e.g., the critical threshold stress) is not accurate for several reasons. The smectic LCE presumably has a higher degree of local order and chain anisotropy,[39] as well as a lower cross-link density and slightly larger domain size. In addition, the measurements of the side-chain, nematic network were performed under thermodynamic equilibrium.

Terentjev and co-workers[22,25,26] assert that the LC polydomain microstructure corresponds to a highly frustrated state of global thermodynamic equilibrium caused by the presence of "random, quenched disorder"[40] in the system possibly due to cross-links, chain entanglements, synthesis defects, etc. A continuum model is formulated from this basis by taking into account the competition between a random, disordering field and an external, aligning field (e.g., a mechanical stress). The resulting predictions given in Figures 20a−c are compared qualitatively with our experimental results. The theory predicts a discontinuous change in a "mean order parameter" (e.g., in our case, the orientation parameter, S) at a critical stress value $\sigma_{threshold}$, and a flattening of the stress-versus-strain curve near $\sigma_{threshold}$,[41] which agrees qualitatively with the experimental results of this study and others. Experiments on LCEs yield a well-developed plateau region in the stress-versus-strain curve rather than a slight flattening, which most likely is due to inhomogeneous deformation as the transition occurs. The characteristic LC domain size, ξ_o, is predicted to remain roughly constant with the applied external field,[42] suggesting that the increase in orientation takes place primarily through the rotation of individual domains rather than by the growth of a few favorably oriented domains. Although we find that there is a substantial elongation of the domains along the stress axis and a corresponding significant increase in domain size, the concept of local director rotation is clearly substantiated (Figure 21). From the POM results of the mechanically oriented LCEs used in this study, it is obvious that the smooth, "delocalized" domain boundaries (disclination brushes) of the unstrained polydomain become sharp, "localized" domain walls in the strained state as predicted.[26] These defects are neither destroyed nor removed from the sample by

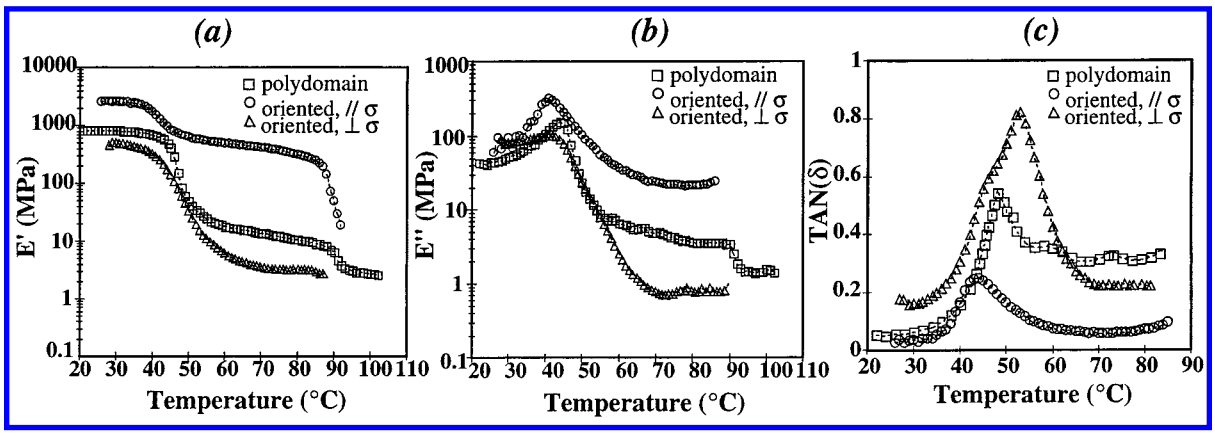

Figure 19. (a) Storage modulus, E', loss modulus, E'', and loss tangent tan(δ), as a function of temperature for the unoriented and mechanically oriented DGDHMS/SA elastomer.

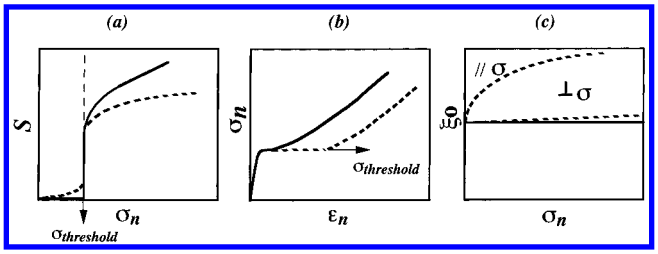

Figure 20. Qualitative predictions of the random field theory[26] as applied to polydomain LCEs (—) compared with experimental trends (- - -); schematics of (a) orientation parameter versus nominal stress, (b) nominal stress versus nominal strain, and (c) characteristic LC domain size versus nominal stress.

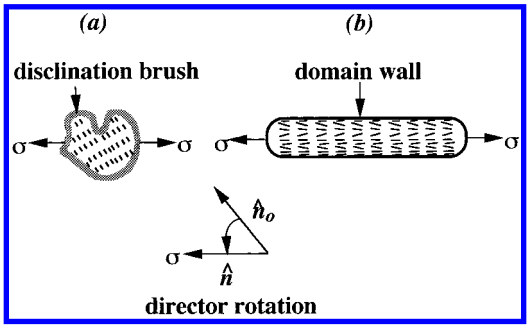

Figure 21. Schematic of the elongation and reorientation of a single smectic LC domain (a) before the application of stress and (b) after the application of stress.

straining. The domains do not deform in an affine manner, i.e., if this were the case, then $d_{//} = d_o\lambda$, where d_o is the original (unstrained) domain size and $d_\perp = d_o\lambda^{-1/2}$ from volume conservation.

Conclusions

We observed a "polydomain-to-monodomain" transition in a smectic, main-chain LCE deformed in uniaxial tension. The σ_n versus ϵ_n and orientation versus σ_n behavior were similar to that reported for side-chain, nematic LCEs[10] and to that predicted theoretically,[26] which suggests that this transition is a universal phenomenon.

Polarized optical microscopy showed that the transition took place by an elongation of the LC domains and a rotation of the local director orientations along the stress axis. Even in the highly oriented "monodomain" samples, orientation was incomplete and many defects were still present running along the tensile axis, indicating that the former smooth, "delocalized" domain boundaries or disclination brushes became sharper, "localized" domain walls.

The deformed smectic samples exhibited an almost complete mechanical hysteresis within the smectic phase, i.e., the strain and orientation were retained on unloading even after annealing above T_g for extended periods of time, as long as $T < T_i$. Upon heating, the oriented samples cleared at approximately the same temperature as the undeformed polydomains and, when subsequently cooled from the isotropic state, "remembered" their original polydomain microstructure and sample dimensions.

Dynamic mechanical analysis shows large differences in mechanical properties between the smectic and isotropic phases and also between oriented and unoriented samples. In particular, the smectic phase exhibits a large storage modulus above T_g, possibly due to the restricted motion of the cross-links within the smectic layers.

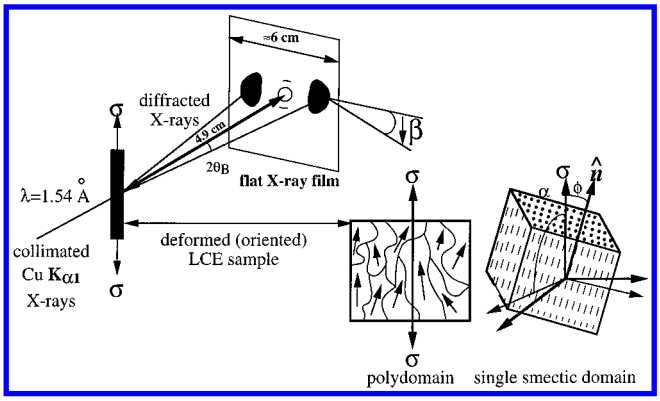

Figure 22. Schematic of wide-angle X-ray diffraction experiment on a deformed polydomain, smectic LCE.

Appendix

1. Calculation of Orientation Parameter, *S*, from WAXD patterns. The experimental setup for conducting WAXD experiments is shown schematically in Figure 22. All of the angles needed for the calculation of *S* and referred to in the following section are also defined in Figure 22. *S* was calculated from azimuthal scans passing through the diffuse, wide-angle reflections by the Hermanns' method[43] using a Fortran program.[44] The distribution in intensity (I) as a function of the azimuthal angle (β) for a given quadrant of the azimuthal scan was obtained, and the intensity maxima were set to an angle of $\beta = 0°$. Conversion of the $I(\beta)$ data to $I(\alpha)$ was accomplished using the relationship from spherical trigonometry:

$$\cos(\alpha) = \cos(\beta)\cos(\theta_B) \tag{4}$$

where θ_B is the Bragg angle and α is the angle between the normal and the scattering planes and the individual domain directors, $\hat{n}$. To calculate the average cosine square of α, integration of the $I(\alpha)$ data versus α was performed using eq 5:

$$\langle\cos^2\alpha\rangle = \frac{\int_0^{\pi/2} I(\alpha)\sin(\alpha)\cos^2(\alpha)\,d\alpha}{\int_0^{\pi/2} I(\alpha)\sin(\alpha)\,d\alpha} \tag{5}$$

From the sample geometry, the summation of the average angles between the x, y, and z axes and the director equals 1. If cylindrical symmetry of the molecular long axis is assumed, one can relate $\langle\cos^2\alpha\rangle$ to the average angle of interest $\langle\cos^2\varphi\rangle$ using eq 6.

$$\langle\cos^2\varphi\rangle = 1 - 2\langle\cos^2\alpha\rangle \tag{6}$$

S can then be calculated from eq 1 and represents the average of the four orientation parameters calculated for each image quadrant.

2. Synthesis of Diglycidyl Ether of 4,4′-Dihydroxy-α-Methylstilbene (DGDHMS) LC Monomer. Five grams (0.0663 mol) of 4,4′-dihydroxy-α-methylstilbene (DHMS), 61.35 g (0.6630 mol) epichlorohydrin, 5.4 g H_2O, and 33 g 2-propanol were added to a reaction flask and heated to 55 °C (bath temperature, 75−80 °C) while stirring under nitrogen. When the bath temperature reached 75 °C, 4.80 g (0.1194 mol) NaOH dissolved

in 19.2 g H_2O are added dropwise during a 40-min period. After completion of the NaOH solution, the reaction mixture was stirred for another 10 min. Stirring was stopped and the aqueous layer pipetted off. After this, stirring was resumed and after a total of 20 min following the completion of the first NaOH addition, a second solution of 2.13 g (0.0528 mol) NaOH in 8.4 g H_2O was added to the reaction mixture for a 20-min period. After completion, stirring was continued for an additional 30 min. The reaction mixture was poured into 100 mL cold H_2O and then 300 mL ice-cold methanol. The clear white product was filtered through a Buechner funnel, washed five times with cold water, and then two times with ice-cold methanol. A clear, white, crystalline product was isolated (yield ≈90%).

Acknowledgment. The authors would like to acknowledge the following people who assisted in polymer synthesis; Jia Shiun-Lin, Audrey Robinson, Dr. Yakhov Freidzon, Dr. Allen Gabor, Dr. Scott Clingman, Dr. Guo Ping Mao, and Dr. Hilmar Koerner. For technical consultation we would also like to thank Dr. Hilmar Koerner, Atsushi Shiota, and Maura Weathers (X-ray diffraction experiments and analysis), Margaret Rich (optical microscopy), Dr. Jan Genzer (image analysis), John Hunt (SEM), and George Chevalier (mechanical testing). For many helpful discussions, we are grateful to Drs. Mark Warner and Eugene Terentjev. This research was sponsored by the National Consortium for Graduate Degrees for Minorites in Science and Engineering (GEM, Inc.), The Department of Education (DOE), and the National Science Foundation (NSF).

References and Notes

(1) For more information on Schlieren and other textures see, for example, Demus D.; Richter L. *Textures of Liquid Crystals*; VCH Publications: New York, 1978. Kléman, M. In *Liquid Crystals and Plastic Crystals*; Gray, G. W.; Winsor, P. A., Eds.; Ellis Horwood Ltd.: Chichester, England, 1974; Vol. 1, p 75. Kléman, M. *Advances in Liquid Crystals*; Academic Press: New York-San Francisco-London, 1975; Vol. 1, p 267. Bouligand, Y. *Defects and Textures in Liquid Crystals: Dislocations in Solids*; Nabarro, F. R. N., Ed. Hudson, S., Ph.D. Thesis, University of Massachusetts, 1990.

(2) See, for example, review articles by Gleim, W.; Finkelmann, H. In *Side-Chain Liquid Crystal Polymers*; McArdle, C. B., Ed., Blackie and Son Ltd.: 1989; p 287. Zentel, R. *Agnew Chem. Adv. Mater.* **1989**, *101* (10), 1437. Barclay, G. G.; Ober, C. K. *Prog. Polym. Sci.* **1993**, *18*, 899−945. Finkelmann, H.; Brand, H. R. *Trends Polym. Sci.* **1994**, *2* (7), 222−226.

(3) See for example, Warner, M.; Terentjev, E. M. *Prog. Polym. Sci.* **1996**, *21*, 853−891.

(4) Hammerschmidt, K.; Finkelmann, H. *Makromol. Chem.* **1989**, *190*, 1089−1101.

(5) Finkelmann, H.; Kock, H.-J.; Gleim, W.; Rehage, G. *Makromol. Chem., Rapid Commun.* **1984**, *5*, 287−293.

(6) Mitchell, G. R.; Coulter, M.; Davis, F. J.; Guo, W. *J. Phys. II* **1992**, *2*, 1121−1132.

(7) Zentel, R.; Benalia, M. *Makromol. Chem.* **1987**, *188*, 665−674.

(8) Barnes, N. R.; Davis, F. J.; Mitchell, G. R.; *Mol. Cryst. Liq. Cryst.* **1989**, *168*, 13−25.

(9) Davis, F. J.; Gilbert, A.; Mann, J.; Mitchell, G. R. *J. Polym. Sci., Part A: Polym. Chem.* **1990**, *28*, 1455−1472.

(10) Schätzle, J.; Kaufhold, W.; Finkelmann, H. *Makromol. Chem.* **1989**, *190*, 3269−3284.

(11) Kaufhold, W.; Finkelmann, H.; Brand, H. R. *Makromol. Chem.* **1989**, *192*, 2555−2579.

(12) Finkelmann, H.; Brand, H. R. *Trends Polym. Sci.* **1994**, *2* (7), 222−226.

(13) Brand, H. R. *Makromol. Chem., Rapid Commun.* **1989**, *10*, 57.

(14) Meier, W.; Finkelmann, *H. Mater. Res. Soc. Bull.* **1991**, *16* (1), 29. Nishikawa, E.; Finkelmann, H. *Macromol. Chem. Phys.* **1997**, *198*, 2531−2550.

(15) Zentel, R.; Reckert, G. *Makromol. Chem.* **1986**, *187*, 1915−1926.

(16) Zentel, R.; Schmidt, G. F.; Meyer, J.; Benalia, M. *Liq. Cryst.* **1987**, *2* (5), 651−664.

(17) Canessa, G.; Reck, B.; Reckert, G.; Zentel, R. *Makromol. Chem., Macromol. Symp.* **1986**, *4*, 91−101.

(18) Bualek, S.; Kapitza, H.; Meyer, J.; Schmidt, G. F.; Zentel, R. *Mol. Cryst. Liq. Cryst.* **1988**, *155*, 47−56.

(19) Giamberini, M.; Amendola, E.; Carfagna, C. *Makromol. Rapid Commun.* **1995**, *16*, 97−105.

(20) Barclay, G. G.; McNamee, S. G.; Ober, C. K.; Papathomas, K. I.; Wang, D. W. *J. Polym. Sci., Part A: Polym. Chem.* **1992**, *30*, 1843−1853.

(21) Shiota, A., Cornell University, unpublished results, 1996.

(22) Clarke, S. M.; Nishikawa, E.; Finkelmann, H.; Terentjev, E. M. *Macromol. Chem. Phys.* **1997**, *198*(1), 3485−3498.

(23) Zhao, Y. *Polymer* **1995**, *36*, 2717−2724.

(24) ten Bosch, A.; Varichon, L. *Macromol. Theory Simul.* **1994**, *3*, 533−542.

(25) Terentjev, E. M. *Proceedings of the NATO Advanced Research Workshop, Manipulation of Organization in Polymers using Tandem Molecular Interactions*; Pisa, Italy, May, 29 − June 2, 1996.

(26) Fridrikh, S. V.; Terentjev, E. M. *Phys. Rev. Lett.* **1997**, *79*, 4661. Terentjev, E. M.; Warner, M.; Verweg, G. C. *J. Phys. II* **1996**, *6*, 1049. Terentjev, E. M. *Europhys. Lett.* **1993**, *23*, 27. Terentjev, E. M. *Makromol. Symp.* **1997**, *117*, 79. Olmsted, P. D.; Terentjev, E. M. *Phys. Rev. E* **1996**, *53*, 2444.

(27) Ortiz, C.; Kim, R.; Rodighiero, E.; Ober, C. K.; Kramer, E. J. *Macromolecules* **1998**, *31*(13), 4074−4088.

(28) Sue, H.-J.; Earls, J. D.; Hefner, Jr., R. E. *Deformation, Yield, and Fracture of Polymers: Proceedings of the 10th Annual International Conference of the Institute of Materials*; Churchill College, Cambridge, UK, April 7−10th, 1997; Chameleon Press Ltd: 1997; pp 129−132.

(29) Earls, J. D.; Hefner, Jr., R. E. European Patent Appl. 0-379-057A2, assigned to the Dow Chemical Company, 1990.

(30) Saunders: K. J. *Organic Polymer Chemistry*, 2nd ed.; Chapman and Hall: London, 1988; pp 424−427.

(31) Genzer, J., Cornell University, image analysis program, 1997.

(32) Treloar, L. R. G. *The Physics of Rubber Elasticity*; Clarendon Press: Oxford, 1975.

(33) Pak, H.; Flory, P. J.; *J. Polym. Sci.: Polym. Phys. Ed.* **1979**, *17*, 1845.

(34) Rivlin, R. S.; Saunders: D. W. *Philos. Trans. R. Soc. London* **1951**, *A243*, 251.

(35) Douglas, J. F.; McKenna, G. B. *Macromolecules* **1993**, *26*, 3282−3288.

(36) Pakula, T.; Zentel, R. *Makromol. Chem.* **1991**, *192*, 2401.

(37) Gallani, J. L.; Hilliou, L.; Martinoty, P.; Doublet, F.; Mauzac, M. *J. Phys. II France* **1996**, *6*, 443−452.

(38) Deeg, F. W.; Diercksen, K.; Schwalb, G.; Brauchle, C.; Reinecke, H. *Phys. Rev. B.* **1991**, *44* (6), 2830.

(39) The chain anisotropy is defined as ($I_{//}/I_{\perp}$) where $I_{//}$ is the persistance length parallel to director and $I_{\perp}$ is the persistance length perpendicular to the director. From ref. 3, ($I_{//}/I_{\perp}$) can be calculated from the spontaneous distortion of a monodomain LCE from the isotropic to LC phase, $\lambda = L/L_o \approx (I_{//}/I_{\perp})^{1/3}$. Mitchell, G. R.; Davis, F. J.; Guo, W. *Phys. Rev. Lett.* **1993**, *71*, 2047 reports on an acrylate, nematic, side-chain LCE with $I_{//}/I_{\perp} \approx$ **1.16**. Kupfer, J.; Finkelmann, H. *Makromol. Chem. Rapid Commun.* **1991**, *12*, 717 reports on a methacrylate, nematic, side-chain LCE with $I_{//}/I_{\perp} \approx$ **2.5**. Brehmer, M.; Zentel, R. *Mol. Cryst. Liq. Cryst.* **1994**, *243*, 353 report on a main-chain, smectic polymalonate LCE with $I_{//}/I_{\perp} \approx$ **15**.

(40) Imry, V.; Ma, S. *Phys. Rev. Lett.* **1975**, *35*, 1399−1401.

(41) Terentjev, E. M., private communication, 1997.

(42) A weak, square root dependence of domain size on the external field is predicted (41) as given by; ξo, ($\sim 1 + kT(\sigma-\sigma_{threshold})^{1/2}/K^{2/3}$), where K is the Frank elastic constant.

(43) Alexander, L. E. *X-ray Diffraction Methods in Polymer Science*, reprint Ed.; Robert A Krieger Publishing Company: Huntington, New York, 1979.

(44) Shiota, A., Cornell University, 1996.

MA971423X